Synthesis, computational and electrochemical characterization of a family of functionalized dimercaptothiophenes for potential use as high-energy cathode materials for lithium/lithium-ion batteries†‡

Yasuyuki Kiya,[ab] Jay C. Henderson,[a] Geoffrey R. Hutchison[a] and Héctor D. Abruña*[a]

Received 14th May 2007, Accepted 3rd August 2007
First published as an Advance Article on the web 28th August 2007
DOI: 10.1039/b707235j

We present a family of a novel class of organosulfur compounds based on dimercaptothiophene and its derivatives, with a variety of functional groups (electron-donating or electron-withdrawing groups) and regiochemistries, designed as potential high-energy cathode materials with sufficient charge/discharge cyclability for lithium/lithium-ion rechargeable batteries. This study uses as a point of departure the electrochemical and computational understanding of the electrocatalytic effect of poly(3,4-ethylenedioxythiophene) (PEDOT) towards the redox reactions of 2,5-dimercapto-1,3,4-thiadiazole (DMcT). The effective redox potentials of these materials exhibited good correlation with the highest-occupied molecular orbital (HOMO) levels predicted *via* computational modeling. Furthermore, the redox reactions of all the compounds studied were electrocatalytically accelerated at PEDOT film-coated glassy carbon electrodes (GCEs), although some materials exhibited higher energy output than others. By using this approach we have identified several compounds that exhibit clear promise as potential cathode materials and have characterized the molecular interactions between the organosulfur compounds and PEDOT film surfaces involved in the electrocatalytic reactions.

Introduction

For over fifteen years, the investigation of sulfur-based polymer cathodes for lithium/lithium-ion batteries, with higher energy density than conventional lithium metal oxide-based cathodes, has garnered much scientific and technological interest.[1–18] A key electrochemical reaction in the field has been the redox chemistry of thiolates (RS^-), which can be oxidized to give the corresponding radical ($RS^\bullet$) which can, in turn, couple to form disulfides (RSSR). For instance, 2,5-dimercapto-1,3,4-thiadiazole (DMcT), which is one of the most promising organosulfur compounds due to its high theoretical capacity (362 A h kg^{-1}), forms a disulfide polymer by coupling reactions of the electrochemically-generated radical species (Scheme 1).

Organic materials also offer the advantage of being relatively low cost and derived from abundant resources, as opposed to conventional lithium metal oxides. Moreover, chemical tunability of organic compounds has made them even more attractive. That is, organic materials can be modified (designed) to give additional chemical and/or electrochemical properties of interest. In addition, the capability of this redox system to capture lithium ions during discharge (due to formation of the thiolate, which subsequently traps the lithium ions) allows their easy incorporation into the so-called "rocking-chair"-type system employed in commercial lithium-ion rechargeable batteries. However, the charge transfer kinetics of both oxidation and reduction of these materials tend to be too sluggish at room temperature for use in viable lithium/lithium-ion batteries.[19,20] In order to accelerate these redox reactions, our group has previously investigated the use of conducting polymers as electrocatalysts and shown that the redox reactions of DMcT can be dramatically accelerated by the conducting polymer poly(3,4-ethylenedioxythiophene) (PEDOT)[15] as well as by polyaniline (PANI).[5] However, composite cathodes, composed of a thiolate compound such as DMcT and a conducting polymer, often exhibit poor charge/discharge cyclability due to dissolution of the reduction products (typically monomer) of the disulfide polymer when an organic liquid electrolyte is employed.[21,22] Therefore, in order for organosulfur compounds to be of practical use (*i.e.*, repeated charge/discharge cycles) as high-energy cathode materials, procedures and/or materials capable of preventing such dissolution must be developed.

In this study, with the aim of designing materials to improve the charge/discharge cyclability of organosulfur compounds, a

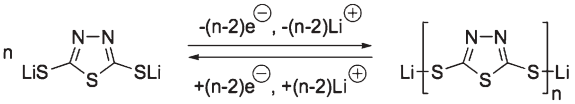

Scheme 1 Redox reaction scheme for 2,5-dimercapto-1,3,4-thiadiazole (DMcT).

[a]*Department of Chemistry and Chemical Biology, Baker Laboratory, Cornell University, Ithaca, New York 14853-1301, USA*
[b]*Subaru Research and Development Inc., Ann Arbor, Michigan 48108, USA. E-mail: hda1@cornell.edu*

† The HTML version of this article has been enhanced with colour images.

‡ Electronic supplementary information (ESI) available: Characterization and synthetic details for the TBT family studied; CVs obtained from electrochemical characterization of the TBT family studied; profile for a PEDOT film cast on ITO electrodes; plots of PEDOT film thickness as a function of charge consumed during the electrochemical polymerization of EDOT. See DOI: 10.1039/b707235j

novel class of organosulfur compounds based upon dimercaptothiophenes[23] (thiophene-2,5-bis(thiolate), TBT), with a variety of functional groups (electron-donating or electron-withdrawing groups) and regiochemistries has been synthesized, and the relationships between the structures and electrochemical activity, as well as the effects of the structures on the electrocatalytic activity of PEDOT towards the redox reactions of these materials, have been investigated. As shown in Fig. 1, these compounds are synthetically tunable, unlike DMcT, and thus offer the promise of covalent bonding either to themselves or to a conducting polymer backbone in order to prevent the materials from leaching into an electrolyte solution during charge/discharge cycles. Moreover, TBT and its derivatives were chosen based on the electrochemical and computational understanding of the thermodynamics of the electrocatalytic effects exhibited by the DMcT/PEDOT system.[15,21,22] Therefore, the electrocatalytic activity of PEDOT towards their redox reactions would be anticipated. From the above-mentioned strategies, this study enabled both the investigation of a class of synthetically-tunable organosulfur compounds, the redox reactions of which should be electrocatalytically accelerated by PEDOT, and further elucidation of the kinetic, thermodynamic and electrocatalytic aspects of reactions between organosulfur compounds and conducting polymers, and thus could lead to future materials that could realize high capacity (and energy) with sufficient charge/discharge cyclability.

The redox behavior of the TBT family and the electrocatalytic activity of PEDOT towards the compounds have been characterized in an AN solution *via* cyclic voltammetry (CV), rotating-disk electrode (RDE) voltammetry, and double potential-step chronoamperometry (DPSCA). The redox behavior of the TBT family, the effect of substituents on the redox behavior of TBT, and the electrocatalytic effect of PEDOT towards the TBT family are discussed in detail. Moreover, chemical interactions between the TBT family and PEDOT, and the effects on the electrocatalytic activity of PEDOT, are also discussed. It was observed that, while the redox reactions of all the compounds were electrocatalytically accelerated when oxidized or reduced at a PEDOT film-modified electrode, as predicted by computational modeling, the electrocatalytic activity of PEDOT differed substantially depending on the specific derivative. Furthermore, several compounds exhibited clear promise as potential energy-storage sites for polymer cathodes for lithium/lithium-ion rechargeable batteries.

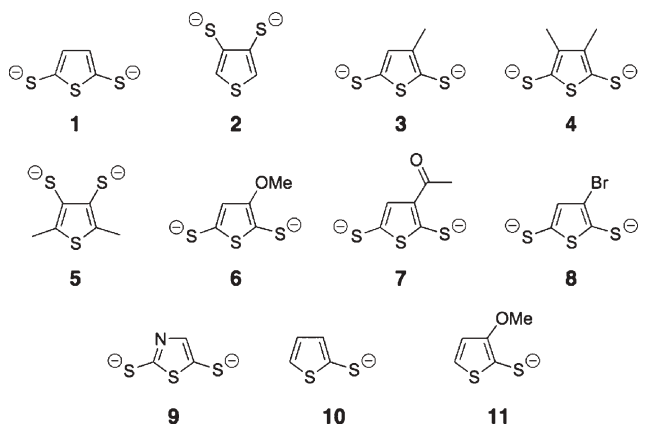

Fig. 1 Organosulfur compounds synthesized and studied, including a variety of electron-donating and electron-withdrawing substituents to the basic thiophene-2,5-bis(thiolate) (TBT) **1** structure: thiophene-3,4-bis(thiolate) (3,4-TBT) **2**, 3-methylthiophene-2,5-bis(thiolate) (methyl-TBT) **3**, 3,4-dimethylthiophene-2,5-bis(thiolate) (3,4-dimethyl-TBT) **4**, 2,5-dimethylthiophene-3,4-bis(thiolate) (2,5-dimethyl-TBT) **5**, 3-methoxythiophene-2,5-bis(thiolate) (methoxy-TBT) **6**, 3-acetylthiophene-2,5-bis(thiolate) (acetyl-TBT) **7**, 3-bromothiophene-2,5-bis(thiolate) (bromo-TBT) **8**, thiazole-2,5-bis(thiolate) (ThiaBT) **9**, thiophene-2-thiolate (TT) **10**, and 3-methoxythiophene-2-thiolate (methoxy-TT) **11**. The acetyl-protected molecules were synthesized to prevent disulfide formation, and the thiolates were generated *in situ* before electrochemical measurements.

Experimental

Dimercaptothiophene and a number of derivatives were synthesized (Fig. 1). Characterization and synthetic details of the dimercaptothiophene family are available in the Supporting Information‡. 2,5-Dimercapto-1,3,4-thiadiazole dilithium salt (DMcT-2Li) was purchased from Toyo Kasei Co. (Japan) and used without further purification. 3,4-Ethylenedioxythiophene (EDOT) was obtained from Bayer Co. (Germany) and used as received. High-purity HPLC-grade acetonitrile (AN) was purchased from Burdick and Jackson, and dried over 3 Å molecular sieves. Lithium perchlorate ($LiClO_4$) (99.99%) and ammonium hydroxide (NH_4OH) (99.99+%) were purchased from Aldrich Chemical Co. Inc., and used as received.

Cyclic voltammetry (CV), rotating-disk electrode (RDE) voltammetry, and double potential-step chronoamperometry (DPSCA) studies were carried out at room temperature using a potentiostat (Hokuto Denko Co., model HSV-100 and HABF1510m) with an analog X–Y recorder (GRAPHTEC Co., model WX4000). In RDE voltammetry studies, linear sweeps were carried out at 5 mV s^{-1} at different rotation rates using a Pine Instrument Co., model AFMSRX rotator. The experimental voltametric profiles were compared to those obtained *via* simulation using DigiSim® version 3.0 (Bioanalytical Systems, Inc. (BAS)). In DPSCA studies, the first potential step was carried out from −1.50 V to +0.80 V and the potential was held at +0.80 V for 60 s. The second potential step was carried out from +0.80 V to −1.50 V and the potential was held at −1.50 V for 60 s. Measurements were taken in a three-electrode cell configuration using glassy carbon electrodes (GCEs) (BAS, 3.0 mm diameter for CV and DPSCA, and Pine Instrument Co., 5.0 mm diameter for RDE voltammetry) as working electrodes, a large area Pt coil counter electrode, and a Ag/Ag^+ (0.05 M $AgClO_4$ + 0.1 M $LiClO_4$/AN) reference electrode without regard to the liquid junction potential, and against which all potentials are reported. The working electrode was polished with 0.3 μm and 0.05 μm alumina slurries (REFINETEC Ltd), rinsed with distilled water and acetone, and dried prior to use. Unless otherwise noted, all experiments were carried out in a 0.1 M $LiClO_4$/AN solution, which was thoroughly purged using pre-purified nitrogen gas.

PEDOT films were prepared on GCEs by anodic electrochemical polymerization of EDOT monomer at a

concentration of 20 mM in a 0.1 M $LiClO_4$/AN solution *via* potential cycling at 20 mV s^{-1} over the potential range from −0.60 and +0.90 V *vs.* Ag/Ag^+.[24] After polymerization, the films were thoroughly rinsed with a 0.1 M $LiClO_4$/AN solution and subsequently used for the characterization of the electrocatalytic activity towards the redox reactions of DMcT-2Li and the dimercaptothiophenes.

Deprotection of the thioacetates to generate the corresponding thiolates was carried out with NH_4OH,[25] producing a combined 25 mL AN solution composed of 50 mM NH_4OH, 1.0 mM of the organothiolate, and 0.1 M $LiClO_4$. In order to complete the deprotection, the solution was left for 3 hours (as discussed below) under an inert atmosphere, followed by immediate characterization of the redox behavior by CV, RDE voltammetry, and DPSCA.

Computational methods

All calculations were performed using the Gaussian 03 program.[26] All compounds were geometry-optimized using density functional theory (DFT) with the B3LYP hybrid functional[27,28] and the 6-31G* basis set, followed by B3LYP single-point calculations using the 6-31++G** basis set for greater accuracy in treating anionic compounds. For comparison, single-point calculations were also performed using B3LYP/6-31++G** using a conductor polarizable continuum model (C-PCM) for an AN solution.[29,30] While HOMO and LUMO eigenvalues from density functional methods cannot be formally taken as either the ionization potential or electron affinity, respectively,[31–34] previous studies have shown that B3LYP-derived eigenvalues compare favorably with experimental electron affinities,[35–40] ionization potentials,[35] and band gaps.[41,42] The differences between the computed HOMO/LUMO values and electrochemical formal potentials are derived from the difference in environments and previous work has shown that solvent effects such as polarizability and cavity radius can be used to linearly adjust (*via* a Kamlet–Taft relationship)[43] computed ionization potentials and electron affinities to compare favorably to electrochemical data.[44]

Results and discussion

We begin with a general discussion of the electrocatalytic cycle between DMcT and PEDOT using electrochemistry and computational modeling of the electronic structure of the species involved. The thermodynamics of the electrocatalytic cycle suggest that some organodisulfide compounds could be similarly electrocatalyzed by PEDOT. We discuss the synthesis of DMcT analogues (*i.e.*, TBT and its derivatives) suggested by computational modeling, the redox behavior of these compounds, and the electrocatalytic activity of PEDOT films modified on GCE surfaces towards the redox reactions of the compounds in solution.

I. Electrocatalytic effect of PEDOT towards the redox reactions of DMcT

Since the redox behavior of thiol compounds at both bare[45,46] and PEDOT film-coated GCEs[21] is strongly affected by the presence of protons (RSH or RS^-), DMcT-2Li was employed in this study to focus solely on the redox behavior of thiolate species and compare the behavior with those of our new dimercaptothiophene family shown in Fig. 1, which was generated *in situ* from the acetyl-protected materials synthesized.[25] Fig. 2b shows a representative CV (obtained at the fifth cycle) for 1 mM DMcT-2Li at a bare GCE in a 0.1 M $LiClO_4$/AN solution. Oxidations of the thiolates to generate the radical species, resulting in the formation of the corresponding dimers and oligomers (polymers) *via* the coupling reactions, were observed over the potential range from −0.60 V to +0.80 V with current peaks at −0.39 V and −0.27 V, and with a corresponding reduction current peak at −0.80 V *vs.* Ag/Ag^+. The very large peak-to-peak separation (>400 mV), ΔE_p, clearly indicates that this redox process is electrochemically irreversible. In addition, the following chemical step (coupling reactions of the radicals) might have an effect on the electrochemical irreversibility. The oxidation peak current, i_p^a, was proportional to the square root of the scan rate, indicating that this is a diffusion-limited process. On the other hand, the fact that the reduction peak current, i_p^c, was directly proportional to the scan rate indicated that the reduction process involved the reductive stripping of a DMcT oligomer film that was generated on the GCE surface during the anodic potential sweep.[21] Furthermore, as anticipated and previously reported,[21,45] it was observed that the oxidation of DMcT-2Li (dithiolate form) was thermodynamically more favorable than that of its dithiol form, DMcT-2H.

Fig. 2a shows a CV for a PEDOT film-coated GCE in a 0.1 M $LiClO_4$/AN solution in the absence of DMcT-2Li. The PEDOT film was obtained by oxidative electropolymerization of EDOT in a 0.1 M $LiClO_4$/AN solution as described in the Experimental section. Over this potential region, p-type doping and dedoping processes were observed as previously reported.[24,47–49] Oxidation of the PEDOT film (doping) started at −1.08 V and a current peak was observed at −0.33 V followed by a plateau current response due mostly to its capacitance.[22] The corresponding reduction (dedoping) current peaks were observed at −0.18 V and −0.84 V, respectively.[50] The oxidation peak current was directly proportional

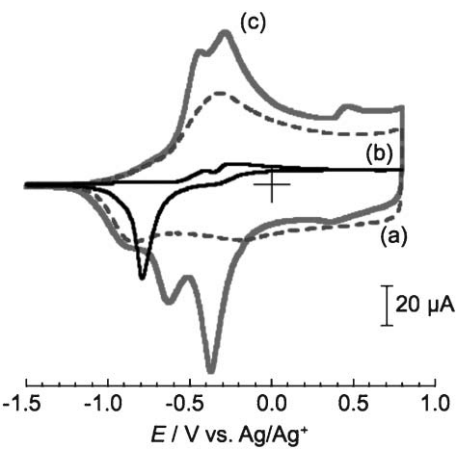

Fig. 2 (a) Representative CV for a PEDOT film-coated GCE in a 0.1 M $LiClO_4$/AN solution. Representative CVs for 1 mM DMcT-2Li at (b) bare and (c) PEDOT film-coated GCEs in 0.1 M $LiClO_4$/AN solutions. The scan rate in all cases was 20 mV s^{-1}.

to the scan rate, indicating that, as would be anticipated, the redox reactions of PEDOT are surface processes and charge propagation is facile.

Fig. 2c shows a representative CV (obtained at the fifth cycle) for a 1 mM DMcT-2Li solution at a PEDOT film-coated GCE in 0.1 M $LiClO_4$/AN. Two oxidation current peaks corresponding to formation of the radical species of DMcT-2Li, resulting in the formation of the corresponding dimers and oligomers (polymers) *via* the coupling reactions, were observed at −0.44 V and −0.28 V, respectively, and the corresponding reduction peaks were observed at −0.63 V and −0.37 V, respectively. This dramatic decrease in ΔE_p points to the high electrocatalytic activity of PEDOT towards the redox reactions of DMcT-2Li as well as those of the doubly protonated DMcT-2H.[15] In addition, the reduction peak (shoulder) observed at −0.89 V was assigned to the reduction of PEDOT. Furthermore, a small redox couple was observed at +0.41 V. This couple is observed reproducibly in 1 mM DMcT-2Li solutions, but not in 5 mM DMcT-2Li solutions under otherwise identical experimental conditions. At this time, we are not certain as to its origin.

II. Computational modeling of dimercaptothiophene and dimercaptothiazole analogues of DMcT

Based on the electrochemical and computational understanding of the thermodynamics of the DMcT/PEDOT electrocatalytic cycle, it would appear that any aromatic organosulfur compound with a HOMO level between the neutral PEDOT HOMO level and cationic PEDOT singly-occupied molecular orbital (SOMO) level should exhibit oxidative electrocatalysis by PEDOT (Fig. 3).[51] Similarly, compounds with a LUMO level approximating the PEDOT HOMO level should show reductive electrocatalysis by PEDOT (Fig. 4). Since the thiadiazole ring in DMcT makes synthetic variations impossible, synthetically modifiable thiazole and thiophene analogues with varying electron-donating and electron-withdrawing substituents were studied in order to establish the applicable range of the PEDOT electrocatalytic cycle to new aromatic organosulfur compounds, as illustrated in Fig. 5. With the exception of dimercaptothiazole **9**, all of the DMcT analogues exhibited very similar orbital energetics to DMcT and thus, the redox reactions of the analogues were anticipated to be electrocatalytically accelerated by PEDOT. As Fig. 5 illustrates, a polymer film of PEDOT is not one homogeneous species with well-defined redox levels, but rather it consists of multiple chain lengths, resulting in energy level broadening. In addition, PEDOT consists both of neutral (unoxidized) and cationic (oxidized) forms.

III. Synthesis of the TBT family

Since it has been reported that dimercaptothiophenes are unstable even for short periods of time at low temperatures[52,53] and handling of thiols can be problematic due to disulfide

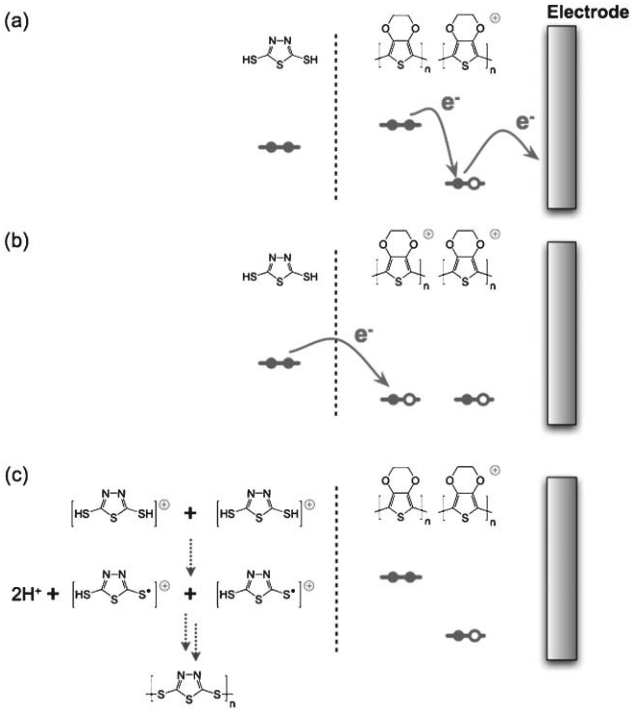

Fig. 3 Schematic of the electrocatalytic cycle between DMcT and a PEDOT film-coated electrode showing the oxidative (charge) processes: (a) neutral EDOT (monomer unit within the PEDOT film) species is electrochemically oxidized, forming $[EDOT]_n^+$ followed by (b) oxidation of the DMcT monomer (or oligomer), regenerating neutral EDOT species followed by (c) proton-coupled polymerization of DMcT monomers (or oligomers) into oligomers/polymers.

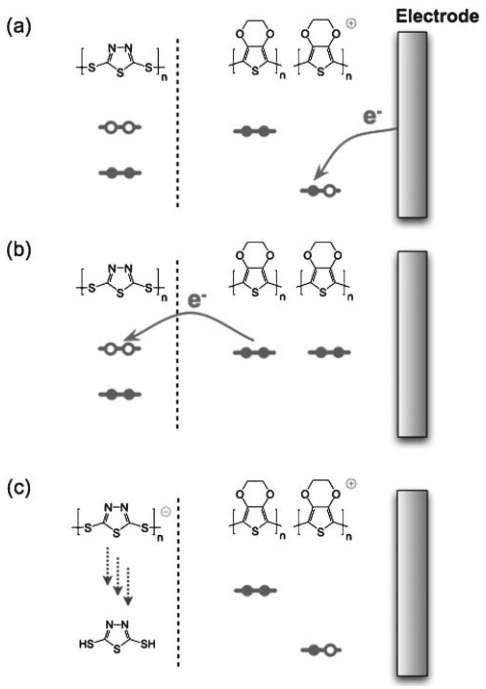

Fig. 4 Schematic of the electrocatalytic cycle between DMcT and a PEDOT film-coated electrode showing the reduction (discharge) processes: (a) cationic EDOT (monomer unit within PEDOT film) species is electrochemically reduced, forming neutral EDOT species followed by (b) reduction of the DMcT oligomers/polymers, regenerating cationic EDOT species followed by (c) proton-coupled disulfide-bond cleavage of DMcT oligomers/polymers into monomers. Note that step (b) is computed to be slightly endothermic, but this is within the accuracy of the method used.

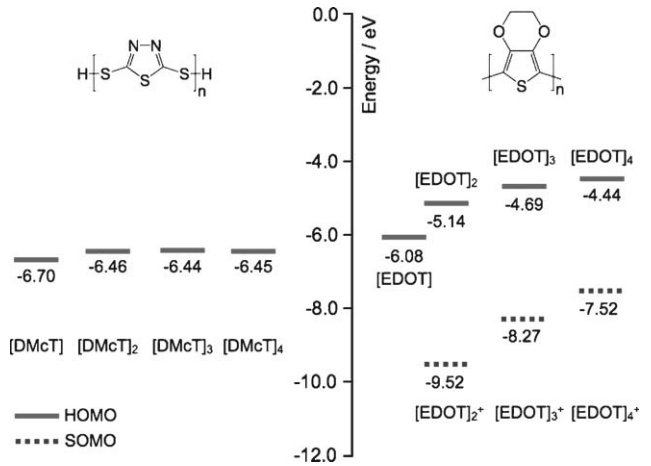

Fig. 5 Computed B3LYP/6-31++G** orbital energies for protonated DMcT and EDOT oligomers, showing relative thermodynamics of the DMcT/EDOT electrocatalyic cycles shown in Fig. 3 and 4.

formation,[53] the protected thioacetate derivatives were synthesized.[54] This protecting group has been widely used for thiols, is known for its facile deprotection, and allows easy isolation, characterization, and storage for long periods of time without decomposition. Characterization and synthetic details can be found in Supporting Information‡.

Previous studies claimed that the N–C–S motifs (*e.g.*, in a thiazole or thiadiazole ring) exhibit faster charge transfer kinetics than C–C–S motifs (*e.g.*, in a thiophene ring).[2,3] Therefore, several attempts were made to synthesize thiazole-2,5-bis(thiolate) **9** and related thiazole derivatives, but the compounds were never isolated. The thiazole compounds are expected to prefer the thione tautomer.[55] Therefore, the electrochemical characterization of the DMcT analogues below is confined to the family of thiophene-bisthiolates **1–8** and thiophene-thiolates **10** and **11**.

IV. Deprotection of thioacetates by ammonium hydroxide and cyclic voltammograms for the TBT family at bare GCEs

Fig. 6b shows a CV for a 1 mM acetyl-protected TBT **1** solution at a bare GCE in 0.1 M $LiClO_4$/AN over the potential range from −1.50 to +0.80 V *vs.* Ag/Ag^+. Protected TBT showed no significant redox responses over this potential range. As expected, upon deprotection, redox reactions of deprotected TBT were clearly observed, as shown in Fig. 6c (the baseline is also shown in Fig. 6a). Similar results were obtained for all compounds in the TBT family. Furthermore, the redox current magnitude did not change significantly between 3–6 hours, although the current response appeared to degrade after significantly longer times (*e.g.* 7–9 hours) (Fig. S1). Thus, it was evident that the protecting groups were cleanly and completely cleaved by NH_4OH within ~3 hours, giving rise to the electroactive dithiolates. In addition, the redox behavior of TT **10**, which possesses a single thiolate group, was compared with that of TBT **1**. Relative to TT, TBT exhibited approximately twice the anodic/cathodic charges, indicating that both thioacetate groups in TBT were cleaved (Fig. S2).

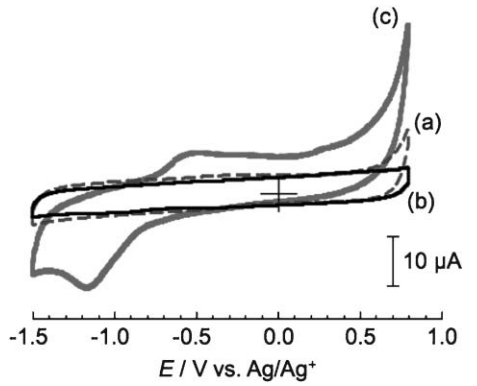

Fig. 6 (a) CV for 50 mM NH_4OH at a bare GCE in a 0.1 M $LiClO_4$/AN solution. CVs for 1 mM acetyl-protected TBT **1** at bare GCEs in 0.1 M $LiClO_4$/AN solutions containing (b) 0 and (c) 50 mM NH_4OH. The scan rate in all cases was 200 m s^{-1}.

Fig. 7 shows CVs for all members of the TBT family **1–8** at bare GCEs in 0.1 M $LiClO_4$/AN solutions containing 50 mM NH_4OH. Since their electrochemical behavior involves multiple oxidative processes (*e.g.*, formation of dimers and oligomers), it is difficult to establish a formal potential, $E^{0'}$, for the oxidation/reduction of the isolated monomer. Therefore, we define an effective formal potential, $E^{\blacksquare}$, as:

$$E^{\blacksquare} = (E_p^{ox} + E_p^{red})/2 \quad (1)$$

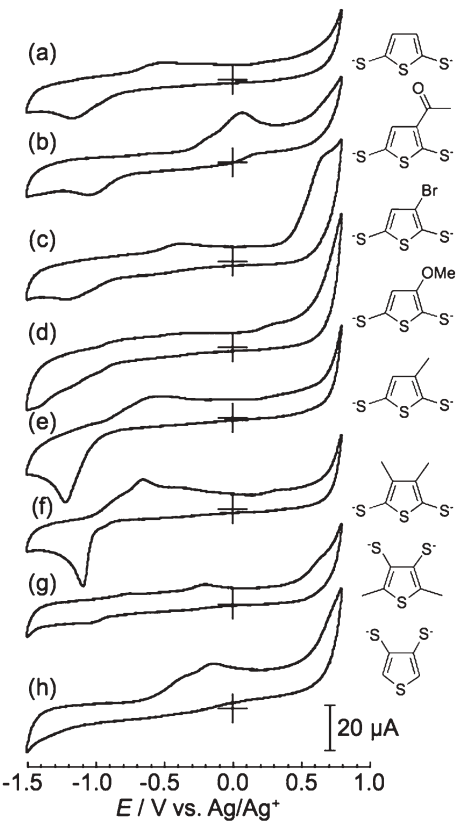

Fig. 7 CVs for 1 mM thiophene-bis(thiolate) monomers at bare GCEs in 0.1 M $LiClO_4$/AN solutions containing 50 mM NH_4OH. The scan rate in all cases was 200 m s^{-1}. Thiophene-bis(thiolate) monomers: (a) TBT **1**, (b) acetyl-TBT **7**, (c) bromo-TBT **8**, (d) methoxy-TBT **6**, (e) methyl-TBT **3**, (f) 3,4-dimethyl-TBT **4**, (g) 2,5-dimethyl-TBT **5**, and (h) 3,4-TBT **2**.

Table 1 Electrochemical and computed properties of the TBT family including peak separation, ΔE_p, effective formal potentials, $E^{\blacksquare}$ (as defined in eqn (1)), and computed DFT HOMO and LUMO orbital energies for dithiolates under the C-PCM solvation model

		Electrochemical		Theoretical	
Compound	Compound number	ΔE_p/V	$E^{\blacksquare}$/V	HOMO/ eV	LUMO/ eV
TBT	**1**	0.66	−0.84	−4.04	0.07
3,4-TBT	**2**	—	—	−4.47	0.06
Methyl-TBT	**3**	0.67	−0.89	−3.97	0.11
3,4-Dimethyl-TBT	**4**	0.42	−0.88	−3.88	0.01
2,5-Dimethyl-TBT	**5**	0.78	−0.59	−4.33	0.04
Methoxy-TBT	**6**	—	—	−4.04	0.01
Acetyl-TBT	**7**	1.11	−0.49	−4.30	−1.05
Bromo-TBT	**8**	0.81	−0.78	−4.21	−0.30

where E_p^{ox} is the potential at the oxidative peak current and E_p^{red} is the potential at the reductive peak current. This effective potential $E^{\blacksquare}$ was used to make comparisons between the redox properties of compounds **1–8** as compiled in Table 1. While we acknowledge that this analysis is not strictly thermodynamically rigorous (due to coupled chemical reactions), comparisons among this restricted group of materials is likely valid if one assumes similar reactions.

In order to elucidate the effects of electron-withdrawing and electron-donating substituents on the redox behavior of TBT, TBT derivatives with acetyl, bromo, methoxy, methyl, and dimethyl substituents were studied. Fig. 7a shows a CV for a 1 mM TBT **1** solution at a bare GCE in 0.1 M $LiClO_4$/AN containing 50 mM NH_4OH. The oxidation and reduction peak potentials were observed at −0.51 V and −1.17 V, respectively, and the resulting effective redox potential was −0.84 V *vs.* Ag/Ag^+. The peak separation of 660 mV indicated that this redox system is electrochemically irreversible at the bare GCE, similar to DMcT-2Li. In the case of an electron-withdrawing group such as acetyl-TBT **7** (Fig. 7b), the oxidation and reduction peak potentials were shifted in the positive direction and the effective redox potential was −0.49 V. In addition, the oxidation peak current of acetyl-TBT was greater than that of TBT. We believe that this difference in the magnitude of the current is due, at least in part, to hydrogen bonding interactions of the acetyl group in acetyl-TBT with surface functional groups (such as hydroxyl) known to be present on the surface of glassy carbon electrodes. Furthermore, in the case of bromo-TBT **8** (Fig. 7c), although the reduction peak potential was not shifted significantly, the oxidation peak potential was shifted in the positive direction (similar to acetyl-TBT), yielding an effective redox potential of −0.78 V. The effective redox potential shifts in the positive direction were consistent with the electron-withdrawing nature of the substituents, as would be anticipated.

For TBT derivatives with electron-donating groups such as methyl-TBT **3** (Fig. 7e) and dimethyl-TBT **4** (Fig. 7f), although the oxidation and reduction peak potential shifts were modest in magnitude, the effective potentials were shifted in the negative direction (−0.89 V and −0.88 V, respectively) consistent with the electron-donating properties of the substituents. On the other hand, in the case of methoxy-TBT **6** (Fig. 7d), no clearly developed oxidation and reduction waves were observed over this potential range.

Next, in order to assess the effects of regiochemistry, the redox behavior of 2,5-dimethyl-TBT **5** (Fig. 7g) was compared to that of 3,4-dimethyl-TBT **4** (Fig. 7f) and 3,4-TBT **2** (Fig. 7h) to TBT **1** (Fig. 7a). Fig. 7g shows a CV for a 1 mM 2,5-dimethyl-TBT **5** solution at a bare GCE in 0.1 M $LiClO_4$/AN containing 50 mM NH_4OH. With the thiolates at the 3,4-positions *versus* the 2,5-positions the reduction peak potential did not shift significantly, but the oxidation peak potential did shift to be more positive, resulting in an increased peak separation and a shift in $E^{\blacksquare}$. Fig. 7h shows a CV for a 1 mM 3,4-TBT **2** solution at a bare GCE in 0.1 M $LiClO_4$/AN containing 50 mM NH_4OH. Compared to the parent compound, TBT **1**, it was observed that the oxidation peak potential shifted in the positive direction and the reduction peak potential shifted in the negative direction, far enough that the reduction current peak was not observed over this potential range. From these increases in the peak separations, therefore, it was deduced that the electron transfer kinetics for the redox reactions of 3,4-dimethyl-TBT and TBT are faster than those of 2,5-dimethyl-TBT and 3,4-TBT, respectively, and indicated that the thiolates at 2,5-positions are more reactive and thus preferred for fast charge/discharge cycles. This effect illustrates the importance of the proximity of the ring heteroatoms to the thiolate (*i.e.*, S–C–S *versus* C–C–S bonding patterns), a point previously indicated by Visco and co-workers.[2,3]

Furthermore, mass transport properties for TBT **1**, acetyl-TBT **7**, methyl-TBT **3**, and dimethyl-TBT **4** were investigated. Table 2 shows diffusion coefficients for the compounds, obtained from plots of the anodic peak current, i_p^a, as a function of the square root of the scan rate for the compounds in 0.1 M $LiClO_4$/AN solutions containing 50 mM NH_4OH. While the values seemed to be reasonable, the value for acetyl-TBT was significantly greater than the others.

V. Comparison of experimental to theoretical results

Since the use of computational modeling suggested that the redox reactions of the entire TBT family (Fig. 1) would be electrocatalytically accelerated at PEDOT film-coated electrodes, it was important to compare the computed gas-phase and dielectric continuum model HOMO energy levels with experimental electrochemical data at bare GCEs. In the dielectric continuum model calculations, the use of computational predictions offers the ability to rationally target novel organosulfur compounds and elucidate the redox properties of the compounds, such as methoxy-TBT **6**, which exhibited little oxidation current at a bare GCE. As illustrated in Fig. 8a, the computed HOMO energy levels in the gas phase showed poor correlation while the dielectric continuum model (Fig. 8b) showed a reasonable correlation with experimental $E^{\blacksquare}$.

Table 2 Diffusion coefficients for TBT **1**, acetyl-TBT **7**, methyl-TBT **3**, and dimethyl-TBT **4**

Compound	Compound number	Diffusion coefficient/$cm^2\ s^{-1}$
TBT	**1**	3.5×10^{-6}
Acetyl-TBT	**7**	1.5×10^{-5}
Methyl-TBT	**3**	4.7×10^{-6}
Dimethyl-TBT	**4**	8.5×10^{-6}

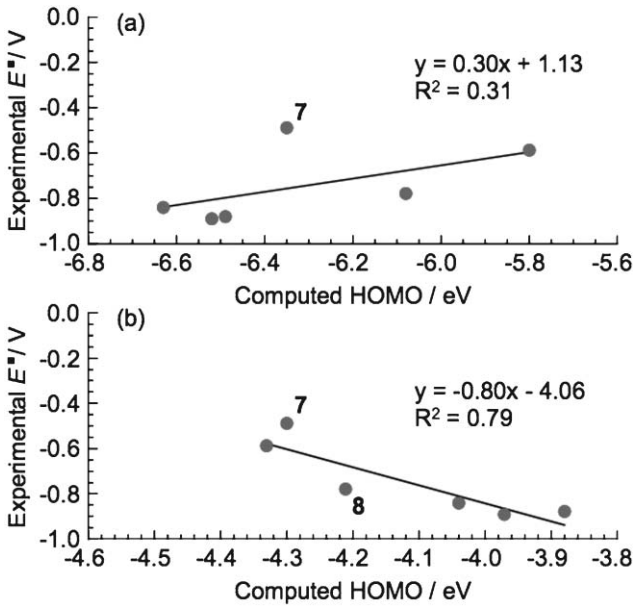

Fig. 8 Comparison between computed B3LYP/6-31++G** HOMO energy levels and experimental $E^{\blacksquare}$ oxidation energies from Table 1 for (a) dithiol (*i.e.*, protonated) compounds in gas-phase, showing low correlation and (b) dithiolates (*i.e.*, deprotonated) using the C-PCM solvation model for AN. The solid lines indicate the best-fit linear regressions with the equations indicated. Note that the largest outliers are the acetyl-TBT **7** species for (a) as well as acetyl-TBT **7** and bromo-TBT **8** species for (b). For the gas-phase oxidation energies in (a), the slope of the trend line is physically incorrect since species with higher computed ionization potentials should have more positive experimental oxidation potentials. On the other hand, the solvation model in (b) indicates a qualitatively correct trend line.

The gas-phase calculations exhibited poor correlation in Fig. 8a because the protonated dithiols showed different conformations of the thiol protons across the series (*i.e.*, coplanar with the thiophene ring *versus* nonplanar), which had a pronounced effect on the computed electronic structure and resulting energies. Consequently, not only were the gas-phase HOMO levels poorly correlated with the experimental $E^{\blacksquare}$ values, but the trend was qualitatively (physically) incorrect, implying that a more negative computed HOMO energy (*i.e.*, large ionization potential) would correlate to a more negative experimental oxidation potential (*i.e.*, easier to oxidize). On the other hand, deprotonated dithiolate compounds exhibited poor correlation between gas-phase HOMO energy levels and experimental electrochemical data because the dianion compounds were poorly described by the gas-phase calculations (*i.e.*, the computed HOMO energies were >0 eV, implying oxidation of the dithiolate in the gas phase was favorable).

In contrast, using the acetonitrile C-PCM solvation model, the calculated HOMO energies were well described and Fig. 8b showed good correlation between the computed HOMO energies and experimental $E^{\blacksquare}$ values. However, it is also worth noting that the correlation includes some error in the experimental $E^{\blacksquare}$ (*i.e.*, an error bar for the *y*-coordinates), which is due to overpotentials involved in the irreversible redox processes at a bare GCE. The largest outliers were acetyl-substituted **7** and bromo-substituted **8** species. Similar trends can be observed for E_p^{ox}, suggesting that even though the electrochemical oxidations are observed to be highly irreversible, this effect is strongly consistent across the TBT family. Additionally, while several of the compounds studied had local minima geometries corresponding to different conformers, the effect on the computed HOMO energies for the dithiolate forms using the C-PCM solvation model was relatively small.

As mentioned above, the main outliers showing relatively poor correlation between the computed solvation energy levels and experimental electrochemical measurements were compounds **7** and **8**. Since conformational effects did not appear to cause significant changes in the computed electronic structure, a likely reason for the differences in computed and experimental values for these species was the distribution of electrostatic charge density, rationalized by π-resonance forms. One resonance form for acetyl-TBT **7** illustrates (see below) how a thiolate group can also exist as a thione resonance form, resulting in increased anionic character on the carbonyl oxygen and decreased anionic charge on the sulfur atom.

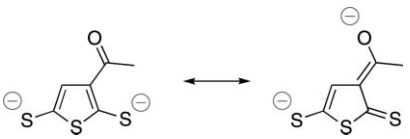

In contrast, although halide substituents exhibit some electron-withdrawing effects, these are mostly σ-inductive, while the π electron density is electron-donating—suggesting a net stabilization of the oxidized form of bromo-TBT **8**. As illustrated in Fig. 8b, bromo-TBT **8** is actually easier to oxidize than was computed (*i.e.*, it lies below the least-squares trend line), while acetyl-TBT **7** is experimentally harder to oxidize than was computed (*i.e.*, it lies above the least-squares trend line). Since the first-principles methods such as DFT implicitly include simple valence-bond resonance pictures as described above, the error is likely due to problems in the treatment of polar solvents interacting with anions in the C-PCM dielectric model.

VI. Characterization of the electrocatalytic activity of PEDOT films towards the redox reactions of the TBT family

The electrocatalytic activity of PEDOT films towards the redox reactions of the TBT family was also characterized by CV, RDE voltammetry, and DPSCA. The potential range employed for CV was from −1.50 V to +0.80 V *vs.* Ag/Ag^+, since the electrocatalytic reactions are expected to occur over the potential region where a PEDOT film is conductive (*i.e.*, in the p-doped state). PEDOT film-modified electrodes exhibited electrocatalytic activity towards both the oxidation and reduction of all the compounds characterized in this study. In this section, we exemplify the electrocatalytic activity of PEDOT films by focusing on the TBT **1** (Fig. 9) and methyl-TBT **3** (Fig. 10) systems, while the rest can be found in the Supporting Information (Fig. S3–S8)‡.

Fig. 9b and 9c present representative CVs for a 1 mM TBT **1** solution at a bare GCE (Fig. 9b) and a PEDOT film-coated GCE (obtained at the fifth cycle, Fig. 9c) in 0.1 M $LiClO_4$/AN

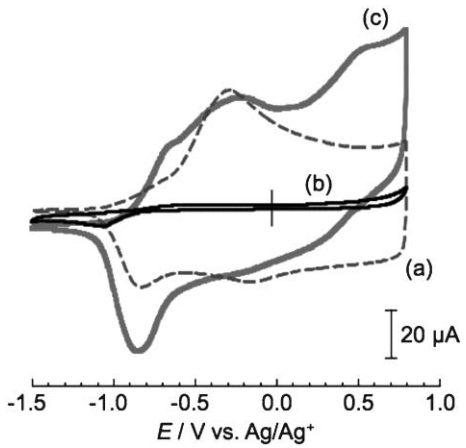

Fig. 9 (a) CV for a PEDOT film-coated GCE in a 0.1 M $LiClO_4$/AN solution. Representative CVs for 1 mM TBT **1** at (b) bare and (c) PEDOT film-coated GCEs in a 0.1 M $LiClO_4$/AN solution containing 50 mM NH_4OH. The scan rate in all cases was 20 m s^{-1}.

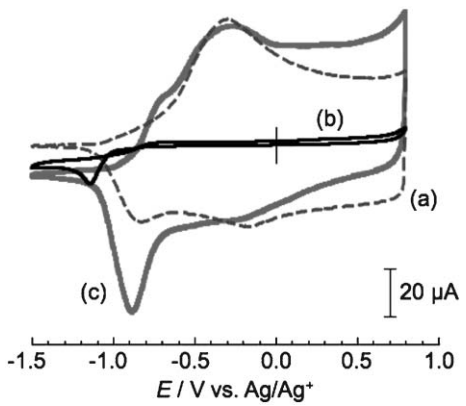

Fig. 10 (a) CV for a PEDOT film-coated GCE in a 0.1 M $LiClO_4$/AN solution. Representative CVs for 1 mM methyl-TBT **3** at (b) bare and (c) PEDOT film-coated GCEs in a 0.1 M $LiClO_4$/AN solution containing 50 mM NH_4OH. The scan rate in all cases was 20 m s^{-1}.

containing 50 mM NH_4OH. Fig. 9a shows a CV for a PEDOT film-coated GCE in a 0.1 M $LiClO_4$/AN solution for comparison. For the oxidation of TBT at a PEDOT film-modified GCE, the onset potential shifted towards negative values and the current response increased relative to a bare GCE. On the other hand, for the reduction, the peak potential obtained at a bare GCE shifted with the increase in the current magnitude from −1.06 V to −0.85 V (ΔE = 210 mV) at a PEDOT film-modified GCE. Thus, PEDOT is capable of electrocatalyzing both the oxidation and reduction processes of TBT as well as DMcT-2Li, as shown previously (Fig. 2). Furthermore, the amount of the increase in the TBT redox current responses is likely smaller than would be found in practical lithium/lithium-ion batteries. In such applications, an organosulfur compound (*e.g.*, TBT) would be incorporated into a composite cathode with PEDOT, rather than freely diffusing towards a PEDOT film from the electrolyte solution as studied in this work. Consequently, these composite electrodes limit the deposition of an insulating layer of TBT polymer over a PEDOT film, which diminishes electron exchange between TBT and PEDOT. Therefore the use of a composite cathode in practical lithium/lithium-ion batteries would retain high electrocatalytic activity of PEDOT and thus higher TBT redox currents.

Fig. 10b and 10c present CVs for a 1 mM methyl-TBT **3** solution at a bare GCE (Fig. 10b) and a PEDOT film-coated GCE (obtained at the fifth cycle, Fig. 10c) in 0.1 M $LiClO_4$/AN containing 50 mM NH_4OH. As was the case for TBT **1**, both the oxidation and reduction reactions were electrocatalyzed at the PEDOT film-modified GCE. For the oxidation (oligomerization process), the current response obtained due to the oxidation of methyl-TBT clearly increased at the PEDOT film-modified GCE. Moreover, the reduction process was greatly electrocatalyzed. This is most evident by noticing the shift in the reduction peak potential from −1.15 V to −0.89 V (ΔE = 260 mV) and the increased current magnitude at −0.89 V.

Next, in order to gain some insight on the charge transfer kinetics of the redox reactions of the dimercaptothiophene compounds at bare and PEDOT film-modified GCEs, the dimerization process of TBT was characterized quantitatively and compared with that of DMcT-2Li using Koutecky–Levich (K–L) plots obtained *via* RDE voltammetry. In these electrochemical kinetics studies, the PEDOT film was treated as an extension of the electrode.[24] We feel that this is a reasonable assumption since in the potential region of interest, the PEDOT film is present in the conducting (p-doped) form. TT **10**, which possesses a single thiolate group, was employed in this study to avoid any complications caused by polymerization process present in TBT. As discussed in Section IV, unlike DMcT-2Li, it is difficult to establish a formal potential for the dimerization of TBT because of the following polymerization process as well as the sluggish charge transfer kinetics.

Fig. 11 shows the K–L plot for the oxidation of TT **10** at a bare GCE in a 0.1 M $LiClO_4$/AN solution containing 50 mM NH_4OH. In this experiment the limiting current, i_L, was measured at −0.25 V *vs.* Ag/Ag^+ at different rotation rates. A Levich plot of i_L *versus* $\omega^{1/2}$ (not shown) exhibited curvature, indicating that the reaction is kinetically limited. A plot of $1/i_L$ *versus* $\omega^{-1/2}$ (K–L plot) was linear, and from the intercept the

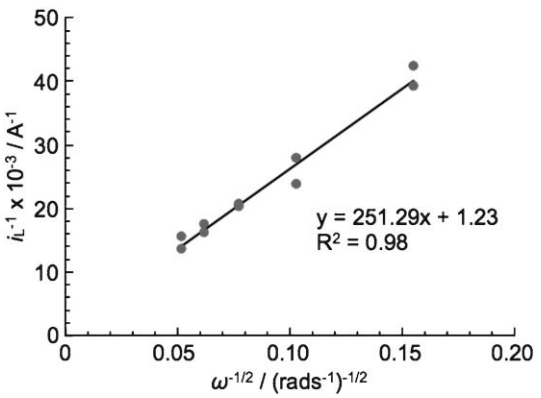

Fig. 11 Koutecky–Levich plot for the oxidation (dimerization) of TT **10** at a bare GCE in a 0.1 M $LiClO_4$/AN solution containing 50 mM NH_4OH. The limiting currents were measured at −0.25 V *vs.* Ag/Ag^+.

kinetically limited current, i_k, was estimated to be 8.1×10^{-4} A. The i_k value includes the rate constant $k(E)$, which is a function of applied potentials. The $k(E)$ value for the dimerization at −0.25 V was determined to be 4.2×10^{-2} cm s^{-1} from which the standard rate constant, k^0, was estimated to be about 2.9×10^{-8} cm s^{-1}. A simulated RDE voltammogram with the same rate constant (2.9×10^{-8} cm s^{-1}), obtained *via* DigiSim®, exhibited behavior quite similar to the experimental data.

Table 3 summarizes the rate constants, determined as described above, for the oxidation (dimerization) of TT and DMcT-2Li at bare and PEDOT film-modified GCEs. The rate constant for the oxidation of DMcT-2Li at a bare GCE was determined to be 6.6×10^{-6} cm s^{-1}. Therefore, at a bare GCE, the dimerization process of DMcT-2Li was found to be ~200 times faster than that of TT. The difference in charge transfer kinetics points to the importance of molecular structure (*i.e.*, thiadiazole *versus* thiophene structures) as well as regiochemistry (dithiolates at 2,5-positions *versus* 3,4-positions) as discussed earlier (see Section IV). At a PEDOT film-modified GCE, k^0 for the dimerization of DMcT-2Li was determined to be 2.9×10^{-4} cm s^{-1}, representing a 44-fold acceleration. On the other hand, k^0 for the dimerization of TT was determined to be 2.7×10^{-6} cm s^{-1}, which represents a 93-fold acceleration. It appears that, while the dimerization process of DMcT-2Li at a PEDOT film-modified GCE is ~100 times faster than that of TT, the electrocatalytic effect of PEDOT is greater (*ca.* 2-fold) towards TT than towards DMcT-2Li.

Finally, in order to compare the electrocatalytic activity of PEDOT towards the redox reactions of TBT, methyl-TBT, dimethyl-TBT, and acetyl-TBT with that towards DMcT-2Li, the anodic and cathodic charges due to redox reactions of the compounds at PEDOT film-modified GCEs were characterized using Anson plots obtained *via* DPSCA. The obtained charges were normalized to the surface coverage (mC cm^{-2}) of PEDOT since it was found that the catalytic activity was proportional to the charge consumed during the electrochemical polymerization of EDOT over the range of charges employed in this study (~180–215 mC cm^{-2}). As a comparison, the normalized charges for the DMcT-2Li/PEDOT system were set to 1 for the anodic and cathodic charges, respectively.

Fig. 12c and 12d present Anson plots for (c) anodic and (d) cathodic reactions of DMcT-2Li at a PEDOT film-coated GCE in a 0.1 M $LiClO_4$/AN solution. Fig. 12a and 12b show Anson plots for (a) anodic and (b) cathodic reactions of the PEDOT film-coated GCE in a 0.1 M $LiClO_4$/AN solution as background responses. The anodic and cathodic charges due to the redox reactions of DMcT-2Li can be estimated by subtracting the redox charge of PEDOT (Fig. 12a and 12b) from the redox charge of the DMcT-2Li/PEDOT system (Fig. 12c and 12d). The anodic and cathodic charges due to the redox reactions of DMcT-2Li were determined to be 1.03 mC and 1.02 mC, respectively, indicating high coulomb efficiency (~99%) at a PEDOT film-modified GCE.

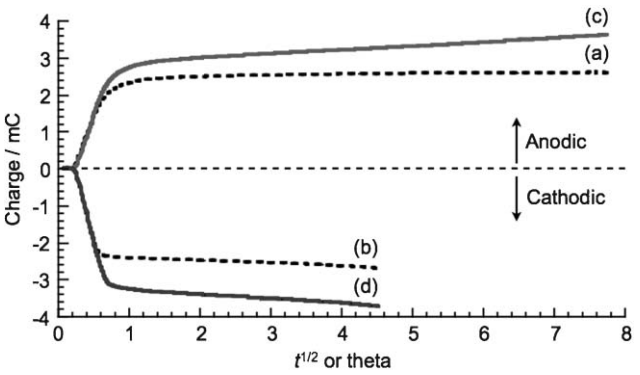

Fig. 12 Anson plots for (a) anodic and (b) cathodic reactions of a PEDOT film-coated GCE in a 0.1 M $LiClO_4$/AN solution. Anson plots for (c) anodic and (d) cathodic reactions of 1 mM DMcT-2Li at a PEDOT film-coated GCE in a 0.1 M $LiClO_4$/AN solution. Theta in the *x*-axis legend is equal to $\tau^{1/2} + (t - \tau)^{1/2} - t^{1/2}$ (τ = 60 s in this experiment).

Table 3 Standard rate constants for the oxidation (dimerization) of TT **10** and DMcT-2Li at bare and PEDOT film-coated GCEs. The transfer coefficient, α, for both reactions was assumed to be 0.5, and an effective formal potential, $E^{\blacksquare}$, was employed (−0.98 V and −0.61 V for TT and DMcT-2Li, respectively) in order to determine the standard rate constants

Compound	$E^{\blacksquare}$/V	Standard rate constant, k^0/cm s^{-1}		Acceleration factor
		At bare GCEs	At PEDOT films	
TT	−0.98	2.9×10^{-8}	2.7×10^{-6}	93
DMcT-2Li	−0.61	6.6×10^{-6}	2.9×10^{-4}	44

Table 4 summarizes the mean normalized charge ratios for the oxidation and reduction of TBT, methyl-TBT, dimethyl-TBT, and acetyl-TBT, compared to the charge obtained for the DMcT-2Li/PEDOT system under identical experimental conditions. The electrocatalytic activity of PEDOT towards the oxidations of the compounds (*i.e.*, the anodic charge) in this family was, in general, greater than that towards DMcT-2Li. On the other hand, the activity towards the reductions (*i.e.*, the cathodic charge) was, in general smaller than DMcT-2Li in most of the trials. Furthermore, the deviations obtained for the anodic charges for the compounds were wider than those for the cathodic charges. For the oxidation process, in which the charge derives from oxidation of the compounds in solution (*i.e.*, a diffusional process), the charge appeared to be more dependent on the morphology of the PEDOT film (the morphology of the electrode surface) rather than its coverage. Indeed, as illustrated in Fig. S9, the PEDOT film is very rough and exhibits significant changes in film morphology from film to film. Consequently, the measured anodic charge was highly variable from trial to trial, and the mean measured anodic charges of the compounds studied were relatively similar.

Upon oxidation, a fraction of the oxidized dimercaptothiophenes is incorporated into the PEDOT matrix, so that upon reduction, the oligomers incorporated into the PEDOT film as well as the ones in solution can be reduced. Thus, the measured cathodic charge can be strongly dependent on the PEDOT coverage. Since the normalization process includes the PEDOT coverage as described above, the cathodic charge shown in Table 4 was highly consistent across trials for a given compound. However, while compounds **1**, **3**, and **4** exhibited normalized cathodic charge ~0.6 times that measured for

Table 4 Mean normalized charge ratios (with standard deviations indicated) for the oxidation and reduction of TBT **1**, methyl-TBT **3**, dimethyl-TBT **4**, and acetyl-TBT **7**, compared to the charges obtained in the DMcT-2Li/PEDOT system under identical experimental conditions

Compound	Compound number	Mean normalized anodic charge ratio	Mean normalized cathodic charge ratio	No. of trials
TBT	**1**	1.51 ± 0.54	0.66 ± 0.08	4
Methyl-TBT	**3**	1.72 ± 0.92	0.69 ± 0.08	3
Dimethyl-TBT	**4**	2.06 ± 0.40	0.59 ± 0.05	3
Acetyl-TBT	**7**	1.93 ± 1.05	0.31 ± 0.05	3
DMcT-2Li	—	1	1	—

DMcT-2Li, compound **7** exhibited a significantly lower value (*i.e.*, ~0.3 times that measured for DMcT-2Li). As described above, the measured cathodic charge can be highly dependent on the amount of reduced oligomers incorporated into the PEDOT film-modified GCE rather than in solution. Therefore, this measurement is, at least in part, indicative of the degree of interaction (whether favorable or unfavorable) between the PEDOT matrix and the oligomeric disulfide compounds.

Since acetyl-TBT **7** exhibited a significantly smaller cathodic charge, it was clear that it experienced a less favorable interaction with the PEDOT film-coated GCE and after oxidation, less of the oligomeric disulfide material appeared to be incorporated into the PEDOT film. As described above (see Section V), an acetyl group has a π-resonance withdrawing effect on the dimercaptothiophene structure, which results in a non-aromatic resonance structure (involving an exo-thione group). Similarly, this resonance structure should have a higher positive partial charge on the thiophene ring as electron density migrates into the acetyl group. The consequence of both effects is an increase in the unfavorable interactions between the acetyl-TBT oligomers and the positively-charged PEDOT film. Higher positive partial charges on the thiophene ring result in unfavorable electrostatic interactions with the positively-charged PEDOT film, and the decreased aromaticity of the thiophene ring decreases favorable π–π interactions. Therefore, it appears that for electrocatalysis between *p*-type conducting polymers and organosulfur compounds, π electron-withdrawing substituents such as an acetyl group are undesirable.

Conclusions

A family of a novel class of organosulfur compounds based on TBT and its derivatives, with a variety of functional groups (electron-donating or electron-withdrawing groups) and regiochemistries, has been synthesized, and its redox behavior as well as the electrocatalytic activity of PEDOT towards the family has been investigated in detail. As anticipated, the effective redox potential ($E^{\blacksquare}$) shifts, determined experimentally for the compounds, were consistent with the electron-donating and electron-withdrawing nature of the substituents. The effective redox potentials of the TBT family exhibited good correlation with prediction *via* computational modeling.

Moreover, the redox reactions of all the compounds synthesized were found to be electrocatalytically accelerated by PEDOT film-modified GCEs, as predicted, based on the understanding of the electrocatalytic cycle exhibited in the DMcT/PEDOT system. Several compounds exhibited clear promise as potential cathode materials for lithium/lithium-ion rechargeable batteries. Therefore, it was found that the rational electrocatalytic cycle predicted *via* computational modeling helped in the design of organosulfur compounds (thiolates) the redox reactions of which can be electrocatalytically accelerated by conducting polymers. Furthermore, the synthetically-tailorable materials prepared in this study would also enable the rational design of additional promising electroactive materials by further chemical modification.

Information about molecular interactions between the TBT family and PEDOT film surfaces, involved in the electrocatalytic reactions, was also obtained in this study. The measured anodic charge, normalized to the PEDOT coverage, was found to be rather variable (from trial to trial) due to the solution measurements employed, which are highly dependent on the morphology of the PEDOT film (the morphology of the electrode surface) rather than its coverage. On the other hand, the measured cathodic charge, normalized to the PEDOT film coverage, was highly consistent for a given compound, since it largely reflects the amount of an oligomeric disulfide compound incorporated into the PEDOT film after oxidation of the thiolate monomers. The electron-withdrawing acetyl substituent exhibits a markedly smaller reduction charge, reflecting an unfavorable interaction between the positively-charged PEDOT film and the acetyl-TBT substrate. This suggests that for p-type conducting polymer electrocatalysts such as PEDOT, electron-donating substituents should be employed to give rise to higher partitioning into the polymer film matrix, and thus provide greater energy output and better charge/discharge cycle performance as cathode materials for lithium/lithium-ion rechargeable batteries.

Acknowledgements

This work was supported in part by the Cornell Center for Materials Research (CCMR), a Materials Research Science and Engineering Center of the National Science Foundation (DMR-0079992) and Fuji Heavy Industries, Ltd (FHI). The authors are grateful to Professor Noboru Oyama (Tokyo University of Agriculture and Technology), Dr Osamu Hatozaki (FHI), Professor Jón T. Njarđarson (Cornell University), and Burak Ülgüt (Cornell University) for helpful discussions. JCH is grateful to Maria Morar (Cornell University) for translation assistance. We are grateful to Professor Dotsevi Y. Sogah and FHI for resources.

References

1 M. Liu, S. J. Visco and L. C. De Jonghe, *J. Electrochem. Soc.*, 1991, **138**, 1891–1895.
2 M. Liu, S. J. Visco and L. C. De Jonghe, *J. Electrochem. Soc.*, 1991, **138**, 1896–1901.

3 M. M. Doeff, S. J. Visco and L. C. De Jonghe, *J. Electrochem. Soc.*, 1992, **139**, 1808–1812.
4 M. M. Doeff, M. M. Lerner, S. J. Visco and L. C. De Jonghe, *J. Electrochem. Soc.*, 1992, **139**, 2077–2081.
5 N. Oyama, T. Tatsuma, T. Sato and T. Sotomura, *Nature*, 1995, **374**, 196–196.
6 E. M. Genies and S. Picart, *Synth. Met.*, 1995, **69**, 165–166.
7 K. Naoi, Y. Oura, Y. Iwamizu and N. Oyama, *J. Electrochem. Soc.*, 1995, **142**, 354–360.
8 P. Novak, K. Muller, K. S. V. Santhanam and O. Haas, *Chem. Rev.*, 1997, **97**, 207–281.
9 K. Naoi, K. Kawase, M. Mori and M. Komiyama, *J. Electrochem. Soc.*, 1997, **144**, L173–L175.
10 L. Yu, X. H. Wang, J. Li, X. B. Jing and F. S. Wang, *J. Power Sources*, 1998, **73**, 261–265.
11 H. Tsutsumi, Y. Oyari, K. Onimura and T. Oishi, *J. Power Sources*, 2001, **92**, 228–233.
12 J. S. Cho, S. Sato, S. Takeoka and E. Tsuchida, *Macromolecules*, 2001, **34**, 2751–2756.
13 H. Uemachi, Y. Iwasa and T. Mitani, *Electrochim. Acta*, 2001, **46**, 2305–2312.
14 L. J. Xue, J. X. Li, S. Q. Hu, M. X. Zhang, Y. H. Zhou and C. M. Zhan, *Electrochem. Commun.*, 2003, **5**, 903–906.
15 N. Oyama, Y. Kiya, O. Hatozaki, S. Morioka and H. D. Abruña, *Electrochem. Solid-State Lett.*, 2003, **6**, A286–A289.
16 X. G. Yu, J. Y. Xie, J. Yang, H. J. Huang, K. Wang and Z. S. Wen, *J. Electroanal. Chem.*, 2004, **573**, 121–128.
17 S. R. Deng, L. B. Kong, G. Q. Hu, T. Wu, D. Li, Y. H. Zhou and Z. Y. Li, *Electrochim. Acta*, 2006, **51**, 2589–2593.
18 M. Amaike and T. Iihama, *Synth. Met.*, 2006, **156**, 239–243.
19 M. Liu, S. J. Visco and L. C. De Jonghe, *J. Electrochem. Soc.*, 1990, **137**, 750–759.
20 S. Picart and E. Genies, *J. Electroanal. Chem.*, 1996, **408**, 53–60.
21 Y. Kiya, G. R. Hutchison, J. C. Henderson, T. Sarukawa, O. Hatozaki, N. Oyama and H. D. Abruña, *Langmuir*, 2006, **22**, 10554–10563.
22 Y. Kiya, A. Iwata, T. Sarukawa, J. C. Henderson and H. D. Abruña, *J. Power Sources*, 2007, DOI: 10.1016/j.jpowsour.2007.04.086.
23 O. Y. Posudievsky, S. A. Biskulova and V. D. Pokhodenko, *Electrochem. Commun.*, 2005, **7**, 477–482.
24 Y. Kiya, O. Hatozaki, N. Oyama and H. D. Abruña, *J. Phys. Chem. C*, 2007, DOI: 10.1021/jp073486f.
25 J. M. Tour, L. Jones, D. L. Pearson, J. J. S. Lamba, T. P. Burgin, G. M. Whitesides, D. L. Allara, A. N. Parikh and S. V. Atre, *J. Am. Chem. Soc.*, 1995, **117**, 9529–9534.
26 M. J. Frisch, G. W. Trucks, H. B. Schlegel, G. E. Scuseria, M. A. Robb, J. R. Cheeseman, J. A. Montgomery, Jr., T. Vreven, K. N. Kudin, J. C. Burant, J. M. Millam, S. S. Iyengar, J. Tomasi, V. Barone, B. Mennucci, M. Cossi, G. Scalmani, N. Rega, G. A. Petersson, H. Nakatsuji, M. Hada, M. Ehara, K. Toyota, R. Fukuda, J. Hasegawa, M. Ishida, T. Nakajima, Y. Honda, O. Kitao, H. Nakai, M. Klene, X. Li, J. E. Knox, H. P. Hratchian, J. B. Cross, V. Bakken, C. Adamo, J. Jaramillo, R. Gomperts, R. E. Stratmann, O. Yazyev, A. J. Austin, R. Cammi, C. Pomelli, J. Ochterski, P. Y. Ayala, K. Morokuma, G. A. Voth, P. Salvador, J. J. Dannenberg, V. G. Zakrzewski, S. Dapprich, A. D. Daniels, M. C. Strain, O. Farkas, D. K. Malick, A. D. Rabuck, K. Raghavachari, J. B. Foresman, J. V. Ortiz, Q. Cui, A. G. Baboul, S. Clifford, J. Cioslowski, B. B. Stefanov, G. Liu, A. Liashenko, P. Piskorz, I. Komaromi, R. L. Martin, D. J. Fox, T. Keith, M. A. Al-Laham, C. Y. Peng, A. Nanayakkara, M. Challacombe, P. M. W. Gill, B. G. Johnson, W. Chen, M. W. Wong, C. Gonzalez and J. A. Pople, *GAUSSIAN 03 (Revision B.04)*, Gaussian, Inc., Wallingford, CT, 2004.
27 A. D. Becke, *J. Chem. Phys.*, 1993, **98**, 5648–5652.
28 C. Lee, W. Yang and R. G. Parr, *Phys. Rev. B: Condens. Matter Mater. Phys.*, 1988, **37**, 785–789.
29 M. Cossi, N. Rega, G. Scalmani and V. Barone, *J. Comput. Chem.*, 2003, **24**, 669–681.
30 V. Barone and M. Cossi, *J. Phys. Chem. A*, 1998, **102**, 1995–2001.
31 J. P. Perdew and M. Levy, *Phys. Rev. B: Condens. Matter Mater. Phys.*, 1997, **56**, 16021–16028.
32 A. Seidl, A. Gorling, P. Vogl, J. A. Majewski and M. Levy, *Phys. Rev. B: Condens. Matter Mater. Phys.*, 1996, **53**, 3764–3774.
33 M. Levy, *Phys. Rev. A: At., Mol., Opt. Phys.*, 1995, **52**, R4313–R4315.
34 R. W. Godby, M. Schluter and L. J. Sham, *Phys. Rev. B: Condens. Matter Mater. Phys.*, 1988, **37**, 10159–10175.
35 C. G. Zhan, J. A. Nichols and D. A. Dixon, *J. Phys. Chem. A*, 2003, **107**, 4184–4195.
36 J. C. Rienstra-Kiracofe, G. S. Tschumper, H. F. Schaefer, S. Nandi and G. B. Ellison, *Chem. Rev.*, 2002, **102**, 231–282.
37 J. C. Rienstra-Kiracofe, C. J. Barden, S. T. Brown and H. F. Schaefer, *J. Phys. Chem. A*, 2001, **105**, 524–528.
38 G. de Oliveira, J. M. L. Martin, F. de Proft and P. Geerlings, *Phys. Rev. A: At., Mol., Opt. Phys.*, 1999, **60**, 1034–1045.
39 L. A. Curtiss, P. C. Redfern, K. Raghavachari and J. A. Pople, *J. Chem. Phys.*, 1998, **109**, 42–55.
40 F. DeProft and P. Geerlings, *J. Chem. Phys.*, 1997, **106**, 3270–3279.
41 J. Muscat, A. Wander and N. M. Harrison, *Chem. Phys. Lett.*, 2001, **342**, 397–401.
42 G. R. Hutchison, *Ph.D. Dissertation*, Northwestern University, Evanston, Illinois, 2004.
43 M. J. Kamlet, J. L. M. Abboud, M. H. Abraham and R. W. Taft, *J. Org. Chem.*, 1983, **48**, 2877–2887.
44 M. Jonsson, A. Houmam, G. Jocys and D. D. M. Wayner, *J. Chem. Soc., Perkin Trans. 2*, 1999, 425–429.
45 E. Shouji, H. Matsui and N. Oyama, *J. Electroanal. Chem.*, 1996, **417**, 17–24.
46 E. Shouji and D. A. Buttry, *J. Phys. Chem. B*, 1999, **103**, 2239–2247.
47 C. Kvarnstrom, H. Neugebauer, S. Blomquist, H. J. Ahonen, J. Kankare and A. Ivaska, *Electrochim. Acta*, 1999, **44**, 2739–2750.
48 G. Zotti, S. Zecchin and G. Schiavon, *Chem. Mater.*, 2000, **12**, 2996–3005.
49 Q. Pei, G. Zuccarello, M. Ahlskog and O. Inganas, *Polymer*, 1994, **35**, 1347–1351.
50 X. W. Chen and O. Inganas, *J. Phys. Chem.*, 1996, **100**, 15202–15206.
51 It should be mentioned that whereas in the electrochemical studies we employed the deprotonated forms of the thiophenes, in the DFT calculations we employed the protonated forms. This was deliberate from our part in an effort to minimize complications in the observed redox response in the former, and the computational difficulties of dealing with anions in the latter. However, we feel that the results from the computations can be compared to the electrochemical ones after taking into account the differences in pH.
52 S. Gronowitz and P. Moses, *Acta Chem. Scand.*, 1962, **16**, 105–110.
53 G. S. Ponticello, C. N. Habecker, S. L. Varga and S. M. Pitzenberger, *J. Org. Chem.*, 1989, **54**, 3223–3224.
54 B. de Boer, H. Meng, D. F. Perepichka, J. Zheng, M. M. Frank, J. Y. Chabal and Z. Bao, *Langmuir*, 2003, **19**, 4272–4284.
55 T. Yamamoto, M. Itoh, N. U. Saitoh, M. Muraoka and T. Takeshima, *J. Chem. Soc., Perkin Trans. 1*, 1990, 2459–2463.

